Liquid Crystals
Publication details, including instructions for authors and subscription information:
http://www.informaworld.com/smpp/title~content=t713926090

Structure formation and its influence on thermodynamic and optical properties of montmorillonite organoclay-5CB liquid crystal nanocomposites

T. Bezrodna[a]; I. Chashechnikova[a]; T. Gavrilko[a]; G. Puchkovska[a]; Y. Shaydyuk[a]; A. Tolochko[a]; J. Baran[b]; M. Drozd[b]
[a] Institute of Physics, NAS of Ukraine, Kyiv 03022, Ukraine [b] Institute of Low Temperature and Structure Research, PAS, Wroclaw 50-950, Poland

To cite this Article Bezrodna, T. , Chashechnikova, I. , Gavrilko, T. , Puchkovska, G. , Shaydyuk, Y. , Tolochko, A. , Baran, J. and Drozd, M.(2008) 'Structure formation and its influence on thermodynamic and optical properties of montmorillonite organoclay-5CB liquid crystal nanocomposites', Liquid Crystals, 35: 3, 265 — 274
To link to this Article: DOI: 10.1080/02678290701830626
URL: http://dx.doi.org/10.1080/02678290701830626

Liquid Crystals,
Vol. 35, No. 3, March 2008, 265–274

Taylor & Francis
Taylor & Francis Group

Structure formation and its influence on thermodynamic and optical properties of montmorillonite organoclay–5CB liquid crystal nanocomposites

T. Bezrodna[a], I. Chashechnikova[a], T. Gavrilko[a], G. Puchkovska[a]*, Y. Shaydyuk[a], A. Tolochko[a], J. Baran[b] and M. Drozd[b]

[a]*Institute of Physics, NAS of Ukraine, 46 Nauki Prosp., Kyiv 03022, Ukraine;* [b]*Institute of Low Temperature and Structure Research, PAS, 2 Okolna St., Wroclaw 50-950, Poland*

(Received 15 August 2007; final form 27 November 2007)

Montmorillonite (MMT) clay modified with octadecylbenzyldimethylammonium chloride (OBDM), B2, and its composites with nematic liquid crystal (LC) 4-pentyl-4′-cyanobiphenyl (5CB), 5CB–B2, with different concentration of the clay (3–8 wt %) were investigated by X-ray diffraction, polarizing optical microscopy, differential scanning calorimetry, FTIR spectroscopy and atomic force microscopy. Modification of Na-MMT with OBDM surfactant results in an increase of the chemical affinity of the clay for 5CB. This results in considerable increase of the basal spacings of the clay, giving a possibility for 5CB dimers to penetrate into the interlayer space. Better affinity of the clay for LC allows clay nanoparticles to disperse homogeneously in the LC, and affects thermodynamic and optical properties of the nanocomposites. For 5CB–B2 composites, the structure formation and the strength of the interface interactions were practically independent on B2 concentration. A comparison with 5CB–B3 composites (B3 is MMT modified with dioctadecyldimethylammonium chloride) revealed that the ability of the clay to form homogeneous structures in the LC and thermodynamic and optical properties of the composites are highly dependent on the chemical nature of the surfactant. Varying the type of the clay mineral modifier, it is possible to develop novel heterogeneous LC nanocomposites with desirable electro-optical properties.

Keywords: LC–clay nanocomposites; montmorillonite; 5CB

1. Introduction

Nanocomposites based on liquid crystals (LCs) and clay nanoparticles have attracted much attention owing to their potential applications for the development, for example, of information recording and storage devices, photonic crystals, opto-electronic equipment, etc. (*1–4*). In such nanocomposite materials, nanoparticles of organo-modified clay minerals have proven to be of high efficiency as an inorganic component (*4–7*). The electro-optical (EO) properties of LC–clay nanocomposites formed from the nematic LC 4-pentyl-4′-cyanobiphenyl (5CB) and organo-montmorillonite nanoparticles have been studied previously (*8, 9*). It was shown that the EO behaviour of these materials depends on the chemical structure of the surfactants used for modification of the montmorillonite (MMT) surface. In addition, it is well established that dielectric, thermodynamic, rheological, EO and other physical properties of ''organic–inorganic'' heterosystems depend on the concentration of the inorganic component (*10–15*). In a previous study (*16*), using a number of experimental techniques, we investigated the concentration effect of organophilic MMT modified with dioctadecyldimethylammonium chloride, DODM, (hereinafter referred to as B3) on the structure formation of the LC–clay composite with 5CB. The strongest interactions between the components in the nanocomposite and the most homogeneous structure were observed at an organoclay concentration, C_{B3}, of 4.5 wt %. As found previously (*8*), the substitution of DODM surfactant in MMT structure with another one, i.e. octadecylbenzyldimethylammonium chloride, OBDM, (hereinafter referred to as B2) leads to significant changes in the EO properties of the corresponding LC–clay nanocomposites. The 5CB–B3 composite shows a small EO memory effect (7%) and a large EO contrast value (300–400) (*9*), whereas the 5CB–B2 composite has a larger memory effect (70–75%) and a relatively small contrast value (*17*), (*8*).

Our B2 and B3 clays contain modifiers of different chemical composition. In the B2 sample, OBDM molecules contain a benzyl group, which probably increases the chemical affinity of MMT to 5CB molecules, which also contain phenyl rings. In the case of DODM molecules (B3 sample) no phenyl rings are present, presumably resulting in a smaller affinity of this organoclay to 5CB. In order to clarify the effect of chemical nature of the surfactant used for MMT modification on interface interactions in the nanocomposites with 5CB, in the present work we

*Corresponding author. Email: puchkov@iop.kiev.ua

ISSN 0267-8292 print/ISSN 1366-5855 online

DOI: 10.1080/02678290701830626
http://www.informaworld.com

carried out comprehensive investigation of 5CB–B2 composites with different concentration of inorganic component, C_{B2}, varying from 3 to 8 wt % using the same experimental techniques as those used previously for 5CB–B3 composites (*16*). A comparison of the data obtained for the two types of the nanomaterials will allow the factors to be identified that affect the structure formation and optical properties of 5CB–MMT nanocomposites. The understanding of the phenomena taking place in these systems will assist in the purposeful development of composites with desired optical characteristics.

2. Materials and experimental methods

MMT clay mineral from the Askan deposit, Georgia, $(OH)_4Si_8Al_4O_{20}{\cdot}nH_2O$, was used as an inorganic component for the LC–clay composites. The Na form of this mineral was modified by OBDM cations, which contain a benzyl group and octadecyl chain in their chemical formula.

The procedures for Na-MMT synthesis, its modification with OBDM surfactant and preparation of composites with 5CB are described in detail elsewhere (*8*). For the present investigations, LC–clay composites containing 3, 4.5, 6 and 8 wt% B2 in 5CB were prepared. 5CB (Merck, 98%) is a nematic LC with nematic-to-isotropic phase transition temperature (T_{NI}) of 308.7 K. In its nematic and isotropic phases, the LC consists of dipole–dipole bonded dimers (*17*) approximately 2.3 nm in length and 0.5 nm in diameter.

The following methods were used to study the composites: small-angle X-ray scattering, atomic force microscopy (AFM), differential scanning calorimetry (DSC), polarizing optical microscopy (POM) and FTIR spectroscopy. Details of sample preparation for the measurements and the descriptions of experimental methods are published elsewhere (*16*). X-ray analysis allowed estimation of the thickness of quasicrystals in polycrystalline organoclay powder according to Scherrer's formula, $L=K\lambda/(\beta\cos\theta)$, where $K=0.9$, β is the full width in radians at half peak maximum and θ is the scattering angle. Upon determining basal spacing values and knowing the thickness of the quasicrystals, the number of platelets per crystal was calculated.

The preparation of the composite samples for the POM investigations was carried out at room temperature, where the 5CB liquid crystal is in a nematic state. The corresponding composite was placed on a surface of an ITO-covered glass plate, and then a similar glass plate was put on the sample. The sample thickness was determined from the size of the spacers (20 μm), which were located between the plates. Photomicrographs of all nanocomposites in polarized light were obtained at room temperature on a Carl Zeiss Peraval Interphako microscope. The magnification was × 500.

AFM was used to investigate the distribution of different clay particles in the organic LC matrix. These experiments were carried out with an Explorer TMX 1010 atomic force microscope (Topometrix Thermo-Microscopes, ATOS GmbH, Germany) at room temperature. The AFM images were obtained by a non-contact method with a Si tip at a cantilever resonant vibration frequency of 162 kHz. A cyclic oligomer, C4770L (Wacker LC-Silicones) (*18*) was used as a substrate, where clay mineral particles were inserted. C4770L compound is a cholesteric LC, the molecules of which consist of phenyl rings and CH_2, CH_3 and C=O groups.

3. Results and discussion

X-ray diffraction experiments

Small-angle X-ray scattering measurements showed that the initial Na-MMT sample has a layered periodicity with an interplanar distance of $d=1.24$ nm (the thickness of the alumosilicate block is of 0.98 nm), which is typical of the Na form of MMT clay (*16*) (Figure 1a). The X-ray diffraction pattern of the modified B2 sample shows two peaks corresponding to $d_1=3.9$ nm and $d_2=1.8$ nm, contrary to the results reported by Ho *et al.* (*19*), where MMT modified with dimethyl(dihydrogenated tallow) ammonium was investigated and only one X-ray peak was observed. The peaks obtained by us, probably, reflect the fact that during the modifying process polyatomic OBDM ammonium cations substitute Na cations in the interlayer space, arranging themselves in two different ways, i.e. nearly perpendicularly and almost planar to the clay layers. The length of the OBDM molecule is 2.6 nm and its diameter is 0.7 nm, and the increase in the interplanar distance for the B2 organoclay compared with that of Na-MMT has approximately the same values. It is worth noting that a similar effect was observed previously for the B3 clay (*16*).

The interplanar distances and the number of alumosilicate platelets in the quasicrystals were calculated using Scherrer's formula for both B2 and B3 samples (see Table 1).

X-ray diffraction studies of 5CB–B2 composites revealed an increase in the d_1 value by 0.5 nm (with the same value of d_2) (Figure 1b) compared with that of dry B2 clay, as was observed previously for the

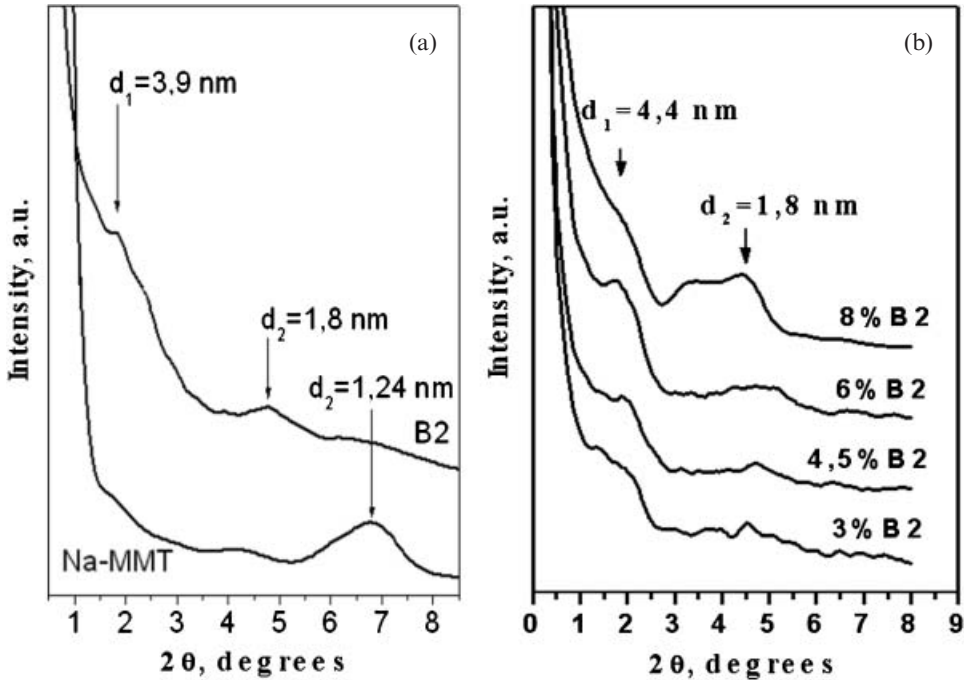

Figure 1. X-ray diffractograms of (a) dry Na-MMT and dry B2 samples and (b) 5CB–B2 composites with clay concentration varying from 3 to 8 wt %.

5CB–B3 heterosystem (*16*). This is probably due to the incorporation of 5CB dimers with a diameter of approximately 0.5 nm into the expanded interlayer space of organically modified MMT. The fact that only the larger lattice period (d_1) increases in the composites at all B2 and B3 (*16*) concentrations compared to dry samples confirms the suggestion mentioned above that two peaks in the modified MMT samples correspond to two types of the interplanar distances (d_1 and d_2), and do not result from first- and second-order reflections of the same layered structure.

POM investigations

Figure 2 shows microphotographs of 5CB–B2 composites with B2 concentrations varying from 3 to 8 wt % (Figures 2a–2d) and a 5CB–Na-MMT sample (4.5 wt %) (Figure 2e), for comparison. In the latter case, organophobic Na-MMT particles are seen to be distributed strongly inhomogeneously, and large domains of homeotropically aligned pure 5CB are observed (black regions in the micrographs). The 5CB–B2 composites show a fairly homogeneous structure, being slightly dependent on B2 clay concentration. In contrast, 5CB–B3 composites were reported to demonstrate a clear dependence of their structure on the B3 concentration, exhibiting the most homogeneous structure at C_{B3}=4.5% (*16*).

Table 1. The interplanar distances and the number of alumosilicate platelets in the quasicrystals of dry initial Na-MMT, B2 and B3 clays.

Sample	Interplanar distance /nm	Number of platelets in a crystallite
Na-MMT	1.24	3–4
B2	3.9	1
	1.8	3
B3	3.6	2
	1.9	3

DSC measurements

DSC was used to trace the effect of B2 concentration on the 5CB nematic-to-isotropic phase transition temperature T_{NI} in 5CB–B2 composites. The rate of heating (cooling) was 8 K min^{-1}. Table 2 shows the DSC data for bulk 5CB and 5CB–B2 composites with B2 concentration varying from of 3 to 8 wt % in both heating and cooling modes. For comparison, the table also lists the corresponding data for the 5CB–B3 composites. For all the 5CB–B2 composites, T_{NI} and T_{IN} are seen to be close and practically do not differ from that of bulk 5CB (within the limits of 1 K). The enthalpy values for the nematic-to-isotropic (isotropic-to-nematic) phase transitions of 5CB in the presence of the B2 particles decrease, whereas their concentration dependences do not have an extreme behaviour. Similarly, a weak concentration dependence of T_{NI} was also reported by other

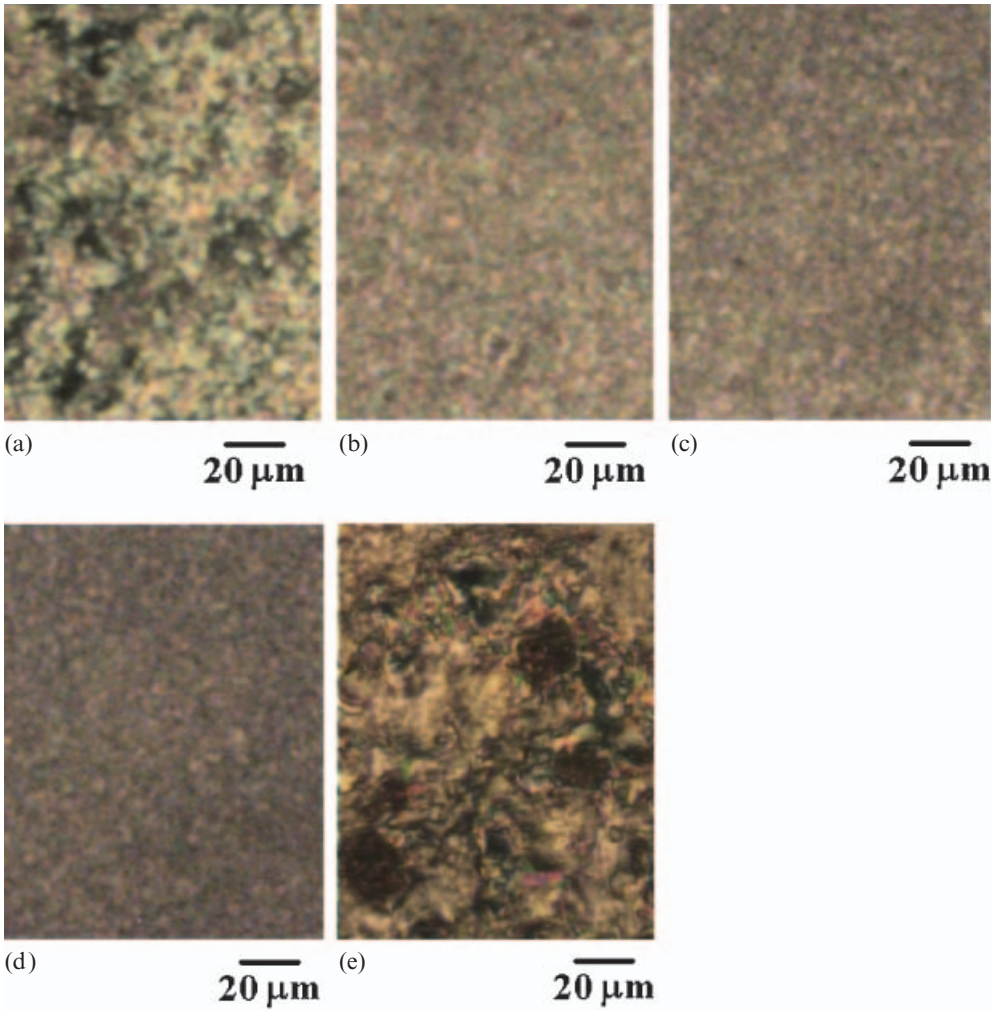

Figure 2. POM photographs of 5CB–B2 composites with B2 concentration of 3% (a), 4.5% (b), 6% (c) and 8% (d), and 5CB–Na-MMT composite (e).

authors for 5CB composites with organoclay (0.5–0.7 K) (*7*) and aerosil (*1, 2*) particles. In contrast, for the 5CB–B3 heterosystem we observed an extreme dependence of the calorimetry parameters on the B3 concentration. The largest decrease of T_{NI} (4.2 K) compared to the bulk 5CB was at C_{B3}=4.5% (*16*). The enthalpy values are also characterised by an extreme behaviour, having their minimum at C_{B3}=4.5–6% (Table 2).

The differences in the types of the concentration dependencies of the T_{NI} (T_{IN}) values and the corresponding enthalpies for the 5CB–B2 and 5CB–B3

Table 2. DSC data for the bulk 5CB and the 5CB–B2 and 5CB–B3 composites.

	Heating		Cooling	
Sample	Enthalpy /J g^{-1}	T_{NI} /K	Enthalpy /J g^{-1}	T_{IN} /K
5CB	2.1	308.7	−2.8	307.8
5CB–B2 (3%)	1.5	308.5	−1.9	306.6
5CB–B2 (4.5%)	1.7	308.7	−2.0	307.3
5CB–B2 (6%)	1.9	307.8	−2.0	306.2
5CB–B2 (8%)	1.5	308.4	−1.6	306.9
5CB–B3 (3%)	2.1	308.3	−2.2	305.0
5CB–B3 (4.5%)	1.4	304.5	−2.0	300.7
5CB–B3 (6%)	1.5	306.1	−1.5	302.2
5CB–B3 (8%)	2.0	309.0	−2.1	306.0

The accuracy in the T_{NI} (T_{IN}) determination is ±0.1 K and in the enthalpy is ±0.2 J g^{-1}.

(Table 2) are connected, probably, with different characters of the structure formation in these nanocomposites, which is in agreement with the POM observations.

FTIR spectroscopy

The mechanism and strength of molecular interactions between the components in 5CB–B2 nanocomposites were investigated by IR spectroscopy for different clay concentrations. Fragments of IR spectra of the B2 organoclay (in comparison with the Na-MMT spectrum), bulk 5CB and 5CB–B2 composites with B2 concentrations of 3, 4.5, 6 and 8 wt % are shown in Figure 3. The IR absorption bands centred at 465 and 520 cm^{-1} are likely to result from Al–O stretching and Si–O–Si bending modes, respectively (*20–22*), and they do not change their peak position after modification of the initial Na-MMT mineral (Figure 3a). The strong broad band at $\sim$1010 cm^{-1} results from in-plane Si–O–Si stretching vibrations, whereas the shoulders centred at 1083 and 1111 cm^{-1} originate from Si–O–Si stretching vibrations perpendicular to the plane of a layer (*22–24*). After Na-MMT modification with organic surfactant, the width of this complex band significantly decreases, and its peak position shifts to 1040 cm^{-1}. At the same time, the intensity of the bands mentioned increases after clay modification with organic surfactant. The spectral changes observed may result from a certain rearrangement of the alumosilicate layers under the incorporation of bulky surfactant molecules into the clay structure. A conclusion involving SiO_4 tetrahedron realignment

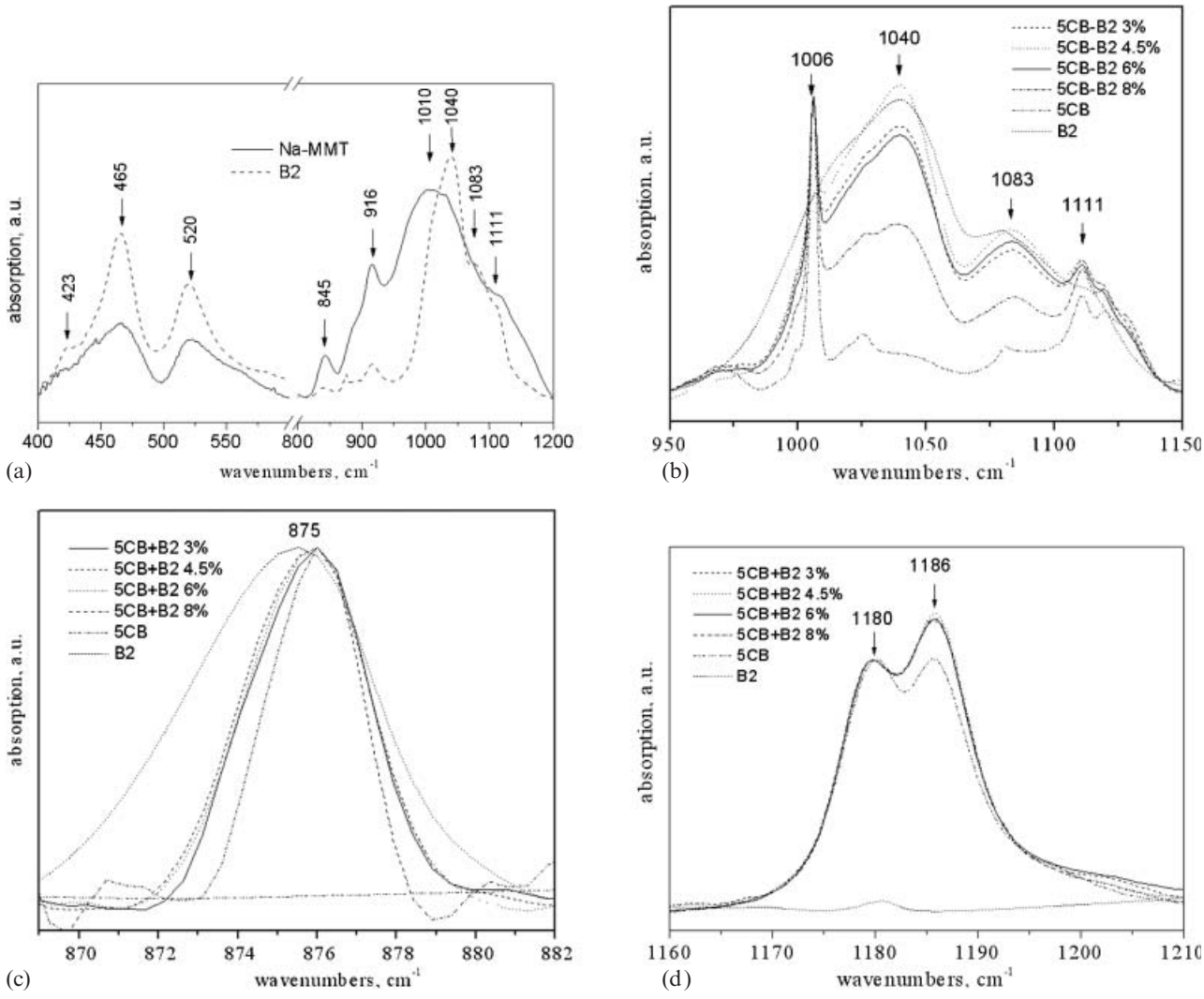

Figure 3. Fragments of IR spectra corresponding to (a) Al–O and Si–O–Si vibrations of the dry clays Na-MMT and B2; (b) Si–O–Si modes in 5CB–B2 nanocomposite compared with that of dry B2 and bulk 5CB; (c) CCH vibrations of OBDM molecules; (d) phenyl ring vibrations in phenyl rings of 5CB molecules.

in the MMT organoclay was proposed by Sontevska *et al.* (*22*) based on spectroscopic changes in the band parameters of Si–O vibrations. Weak absorption bands centred at 845 and 913 cm^{-1} are ascribed to the librational OH vibrations on the MMT surface (*25*).

In the IR spectra of 5CB–B2 nanocomposites with different B2 content (Figure 3b), the peak positions of these bands remain the same, but their significant narrowing by 2–3 cm^{-1} is observed. This may result from the alignment of the near-surface layers of organoclay lamellae under the influence of surrounding 5CB dimers. It worth mentioning that the narrowing of relevant IR absorption bands in the spectra of 5CB–B2 composites is larger than in the spectra of 5CB–B3, which suggests stronger interface interactions in the 5CB–B2 system. At the same time, 5CB–B2 composites do not practically demonstrate a concentration dependence of the spectral widths of the IR absorption bands mentioned. This is contrary to the behaviour reported (*16*) for 5CB–B3 composites, where the minimum bandwidth was observed at B3 clay concentration C_{B3}=4.5%. The width of IR absorption band centred at ~875 cm^{-1}, assigned to out-of-plane C–C–H vibrations of the OBDM monosubstituted phenyl ring (*26*), also considerably decreases. The largest variation in the width of this band is observed for the composites with the largest B2 concentration (8 wt %) (Figure 3c). The above mentioned results suggest that interaction of 5CB molecules with the OBDM ones on the B2 nanoparticle surface occurs via π-electron cloud of the OBDM molecules. Noticeable narrowing of the 875 cm^{-1} band confirms our hypothesis about better affinity of the B2 organoclay for 5CB molecules than that of the B3 organoclay, which has no phenyl rings in its structure.

In the middle-frequency IR spectral region (1100–2400 cm^{-1}), absorption bands corresponding to deformation vibrations of phenyl rings (1180 and 1186 cm^{-1}) (Figure 3d), C=C (1606 cm^{-1}) and C≡N (2226 cm^{-1}) stretching vibrations are observed. The high-frequency IR spectral range (2800–3100 cm^{-1}) contains CH stretching vibrations of CH_2 and CH_3 groups (Figure 4a) and aromatic CH stretching (Figure 4b) of 5CB molecules (*27*). In this spectral range, corresponding vibrations of OBDM molecules are also located. However, taking into account small values of B2 nanoparticles concentration in the nanocomposites, the contribution from OBDM vibrations to the overall spectral shape is very weak and could be neglected.

The presence of B2 nanoparticles practically does not affect the peak positions of IR absorption bands of 5CB or OBDM molecules, which provides evidence for the van der Waals character of the molecular interactions in the composites. The narrowing of spectral bands assigned to C⋯C and C≡N stretching vibrations, as well as C⋯C–H bending vibrations of 5CB biphenyl groups suggests hindering of 5CB reorientations around *x* and *y* molecular axes. This is probably caused by confinement of 5CB molecules between the aliphatic chains of OBDM surfactant on the surface of B2 nanoparticles. In other words, due to molecular van der Waals interactions in the LC–clay composites, an alignment of the LC near-surface layers occurs.

Similar to the behaviour reported for 5CB–B3 composites (*16*), the incorporation of B2 nanoparticles into the 5CB changes the intensity ratio of IR

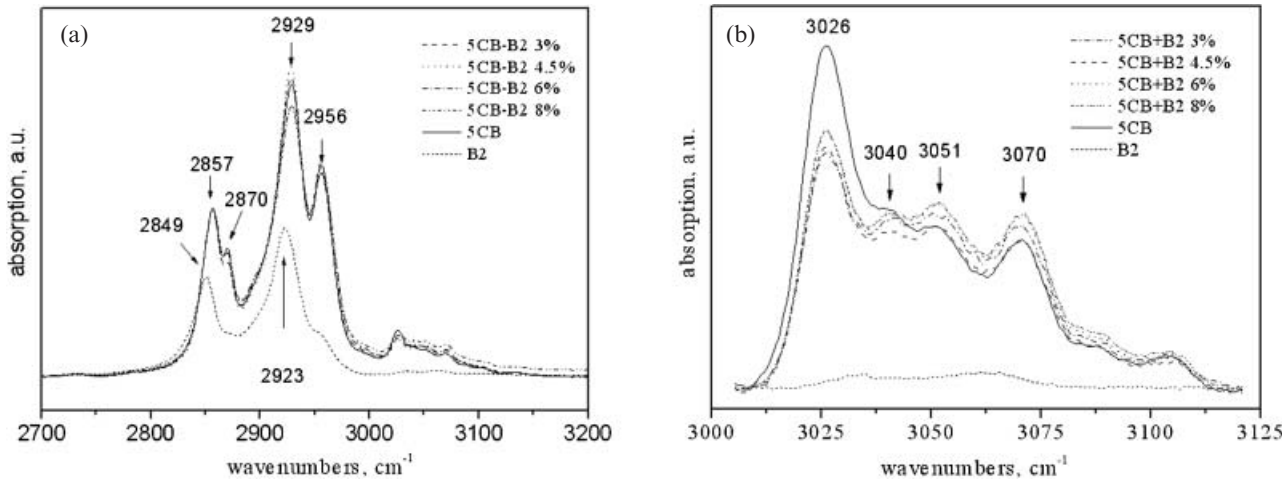

Figure 4. Fragments of IR spectra corresponding to CH stretching of CH_2 and CH_3 groups (a) and aromatic CH stretching (b) vibrations of 5CB molecules.

absorption bands centred at 1186 and 1180 cm^{-1}, which are assigned to phenyl rings bending vibrations in 5CB molecules (Figure 3d). The spectra shown in Figure 3d are normalized against the 1180 cm^{-1} absorption band. According to Babkov *et al.* (*27*), the first of these doublet bands is assigned to the vibrations of the phenyl ring close to the pentyl group, and the second one to the phenyl ring bonded to a CN group. However, contrary to the LC–clay composites with B3 nanoparticles, in the spectra of 5CB–B2 composites, the intensity ratio of these two bands does not depend on B2 concentration. The increase in the intensity of the 1186 cm^{-1} band in the IR absorption spectra of 5CB–B2 nanocomposites as compared with that of bulk 5CB may result from electron density redistribution in corresponding phenyl ring due to its closeness to the polar CN group, which may be involved in electrostatic interaction with residual ions on the clay surface.

The IR absorption bands observed in 2800–3100 cm^{-1} spectral range (Figure 4a) correspond to asymmetric (2956 cm^{-1}) and symmetric (2870 cm^{-1}) C–H stretching of CH_3 groups. The bands centred at 2929 and 2857 cm^{-1} are assigned correspondingly to asymmetric and symmetric C–H stretching of CH_2 groups of the surfactant or 5CB molecules. These absorption bands were shown to be very sensitive to the structural changes of 5CB–B3 composites, being dependent on the clay concentration (*16*). According to Figure 4a, the peak positions of CH_2-group stretching vibrations in the spectra of the 5CB–B2 composite are shifted from their respective values in the spectra of dry B2 by 6–8 cm^{-1}, much as was observed in the spectra of 5CB–B3 composites. However, contrary to the latter, the composites with B2 do not demonstrate a concentration dependence of the intensity ratio of the IR absorption bands related to C–H symmetric and asymmetric stretching vibrations of CH_2 and CH_3 groups.

The IR absorption bands assigned to aromatic C–H stretching vibrations in 5CB molecules (the bands centred at 3026 and 3070 cm^{-1}) do not change their position due to a presence of B2 nanoparticles, and their intensity ratio first markedly decreases already at $C_{B2}=3$ wt %, remaining almost the same with an increase of the organoclay concentration up to 8 wt %. It worth mentioning that in contrast, 5CB–B3S composites demonstrated a clear minimum in the intensity ratio of indicated IR absorption bands at $C_{B3}=4.5$ wt %.

Thus, the analysis of spectral changes in the parameters of IR absorption bands corresponding to the vibration of clay crystal lattice, LC and surfactant molecules indicates that molecular interactions in 5CB–B2 composites result in mutual influence of the components, which appears as an alignment of the near-surface layers at the interface between the organic and inorganic phases. It follows from the above results that molecular interactions are stronger in 5CB–B2 composites than in 5CB–B3, and in the case of 5CB–B2 composites, the concentration dependence of C–H stretching bands intensity ratio does not have an extreme variation, contrary to that observed for 5CB–B3 composites (*16*).

Thus, by comparing IR spectroscopic results obtained in this work for 5CB–B2 composites with corresponding results obtained earlier for 5CB–B3 composites (*16*), we can conclude that molecular interactions between the 5CB and clay nanoparticles are somewhat stronger for the B2 clay than for B3. On the other hand, according to DSC results, addition of B3 nanoparticles causes considerable lowering of T_{NI} of the nematic LC, which suggests that B3 particles disturb the nematic ordering more efficiently than B2, the latter having practically no effect on T_{NI} value. In order to find an explanation for the seeming disagreement between the results obtained by the IR spectroscopy and DSC, we used the AFM method.

AFM measurements

AFM was used to study the morphology of the LC–clay nanocomposites and to estimate the size of the clay particles. The samples for AFM measurements were prepared by application of the organically modified clay powder on mica substrate coated with glass-forming cholesteric LC (cyclic oligomer C4770L, Wacker LC-Silicones). This LC was heated to the clearing temperature and then cooled down to the room temperature, when it hardened. We chose this LC from a set of the compounds, suitable as a substrate for the AFM experiments, since the chemical composition of C4770L, a cyclic oligomer with biphenyl fragments and lateral alkyl chains (*18*), is comparable with that of 5CB. This, probably, allows us to suggest similarities in the effects of the organoclay particles on these two LC textures.

AFM data imaging the suspensions of B2 and B3 particles in the C4470L are shown in Figure 5. In the case of B2 suspension (Figure 5a), the clay particles of 10 nm in height and nearly 100 nm in length are homogeneously distributed in the organic medium. Their aggregation does not occur because of a strong adhesion between the LC and the B2 clay. Small B2 clay particles are located at distances of about 500–800 nm from each other, and their presence does not disturb the LC texture. Probably, due to high chemical and adsorption affinity of the B2 clay to the LC, the energy of interface interactions are large

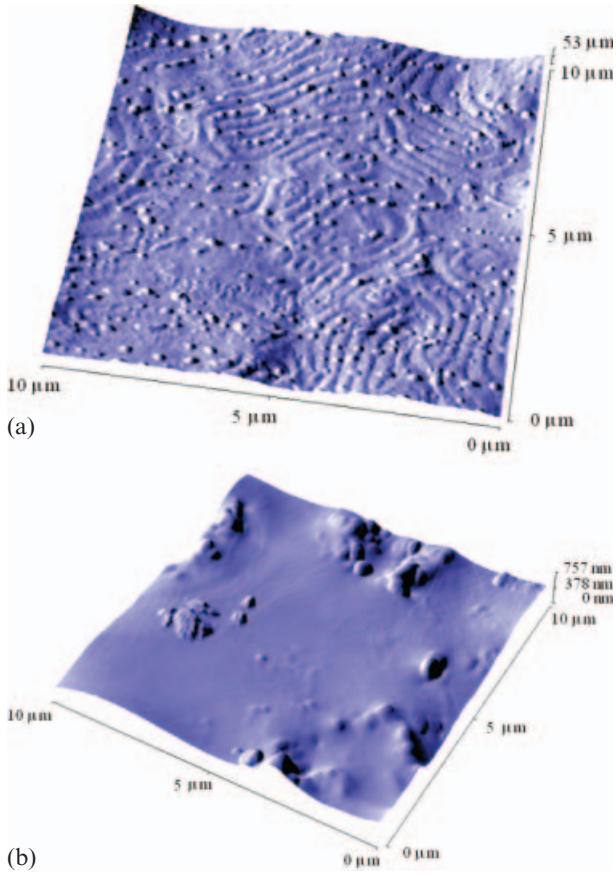

Figure 5. AFM images of clay particles immersed in LC matrix: B2 (a), B3 (b).

enough for the clay particles to be completely covered with a thin layer of the LC, thus preventing their aggregation.

As can be seen from the AFM images (Figure 5b), B3 organoclay particles in the LC are aggregated in a large-scale structure sized from 300 to 1000 nm, which are inhomogeneously distributed in the organic matrix. This occurs due to the poorer affinity of the B3 organoclay for the LC, as compared with that of the B2 clay. In other words, in the case of B3 particles, cohesion between the clay particles (their conglutination) dominates over their adhesion. No cholesteric LC texture is observed for LC–B3 suspensions, which suggests strong disturbing action of the aggregated clay particles on the LC ordering.

From the analysis of AFM data and IR spectroscopy results, we can explain why the B3 clay particles interact more weakly with 5CB molecules than the B2 (as follows from IR spectroscopy data), having a stronger effect on T_{NI} of the LC. This may occur due to strong distortion of the nematic ordering of the LC in the whole volume of the 5CB–B3 composite, where T_{NI} is measured with the DSC method. As is evidenced by the AFM images, small quasicrystals of B2 are completely covered with a thin layer of LC, promoting stronger molecular interaction and additional alignment of 5CB molecules in the near-surface layers (as was evidenced by IR spectroscopy). The ordering of the LC matrix as a whole is not disturbed, so T_{NI} values for the 5CB–B2 composites are close to that of bulk 5CB.

The data obtained suggest that the chemical nature of the surfactant used for clay modification is responsible for chemical affinity between the organoclay particles and LC, which has a strong effect on the structure formation in the LC–clay composites. These properties can also explain different EO characteristics of 5CB composites with B2 and B3 nanoparticles. In the first case, a suspension of well-separated small B2 particles uniformly distributed in the 5CB medium is formed, as confirmed by POM micrographs and AFM images. Under applied electric field, this mobile system is easily oriented along the field direction resulting in significant increase in optical transparency of the 5CB–B2 composite, when the applied voltage increases. Due to the fairly strong molecular interactions in the near-surface layers of the components in the composite, the field-induced alignment of 5CB domains remains the same even when the electric field is

removed, i.e. the system shows a considerable EO memory effect (*8*). This feature of the LC–clay nanocomposites is important for the development of the information storage devices.

In contrast, due to the smaller affinity of DODM molecules to 5CB molecules, B3 particles are only partially covered by LC layer, which allows them to aggregate, and in the 5CB–B3 composites the cohesion forces predominate. These aggregated particles form a stable colloidal spatial network with 5CB dimers. As we have shown in our previous work (*16*), for this composite the structure homogeneity depends on the particle concentration, which is characteristic of the gel-formation processes. The viscosity of 5CB–B3 composites is significantly higher than that of 5CB–B2 and no sedimentation of the mixture is observed in several months. In its initial state this fairly dense composite shows strong light scattering and its optical transmission value is low. In EO measurements, when an electric field is applied to the composite, its transparency increases, but to less of a degree than that in 5CB–B2 composites. The optical memory effect of 5CB–B3 composite is low, but the contrast between the light scattering and transparent states is high (*9*). This feature of the composite is important for the development of the information display devices.

In addition, it worth mentioning here the effect of the exchangeable cations on the phosphorescence properties of benzophenone in the B2 and B3 clay dispersions reported by Gavrilko *et al.* (*28*). As was shown by Gavrilko *et al.* (*28*), organoclay nanoparticles in dispersions are covered with thin amorphous benzophenone layer, the thickness of this layer being smaller for B2 nanoparticles than for B3. Smaller thickness of amorphous benzophenone layer promotes excitation energy transfer from benzophenone molecules to the clay, and more efficient phosphorescence quenching.

4. Conclusions

The 5CB–B2 (3–8 wt %) composites and dry B2 organoclay were investigated by small-angle X-ray scattering, POM, DSC, IR spectroscopy and AFM methods. The experimental results obtained on 5CB–B2 nanocomposites, and their comparison with similar results obtained earlier on 5CB–B3 nanocomposites, showed that the strength of molecular interactions between the clay and the LC are highly dependent on the type of organic surfactant used for clay modification. Modification of Na-MMT with OBDM organic surfactant molecules results in an increase of the chemical affinity of the clay mineral for 5CB nematic LC. In addition, this results in considerable increase of the basal spacings of the clay, giving a possibility for 5CB dimers to penetrate into the interlayer space. In turn, better affinity of the clay for LC allows clay nanoparticles to disperse homogeneously in the LC, and affects thermodynamic (e.g. T_{NI} value) and optical properties of the nanocomposites. For 5CB–B2 composites, the structure formation and the strength of the interface interactions were found to be practically independent on B2 concentration. A comparison with the corresponding data obtained previously for 5CB–B3 composites shows that the ability to form homogeneous structures in the LC and thermodynamic and optical properties of the composites are highly dependent on the chemical nature of the surfactant used for modification of the clay. Varying the type of the clay modifier, it is possible to develop new heterogeneous LC nanocomposites with predicted desirable EO properties.

Acknowledgements

This work was partially funded by the NAS of Ukraine under the Program ''Nanophysics and nanoelectronics'', project VC-138 and under the Program ''Nanomaterials, Nanosystems and Nanotechnologies'', project 10/07-n. The authors would like to thank Dr. Anton Hauser for his help with AFM measurements.

References

(1) Kang D.; Maclennan J.; Clark N.; Zakhidov A.; Baughman R. *Phys. Rev. Lett.* **2001**, *86*, 4052–4055.
(2) Diorio N.; Fisch M.; West J. *J. appl. Phys.* **2001**, *90*, 3675–3678.
(3) Puchkovska G.; Reznikov Y.; Yakubov A.; Yaroshchuk O.; Glushchenko A. *J. Mol. Struct.* **1997**, *404*, 121–128.
(4) Kawasumi M.; Hasegawa N.; Usuki A.; Okada A. *Appl. Clay Sci.* **1999**, *15*, 93–108.
(5) Kawasumi M.; Hasegawa N.; Usuki A.; Okada A. *Liq. Cryst.* **1996**, *21*, 769–776.
(6) Kawasumi M.; Usuki A.; Okada A.; Kurauchi T. *Mol. Cryst. liq. Cryst.* **1996**, *281*, 91–103.
(7) Zhang Z.; Duijneveldt J. *Soft Matter* **2007**, *3*, 596–605.
(8) Chashechnikova I.; Dolgov L.; Gavrilko T.; Puchkovska G.; Shaydyuk Y.; Lebovka N.; Moraru V.; Baran J.; Ratajczak H. *J. Mol. Struc.* **2005**, *744–747*, 563–571.
(9) Bezrodna T.; Chashechnikova I.; Dolgov L.; Puchkovska G.; Shaydyuk Y.; Lebovka N.; Moraru V.; Baran J.; Ratajczak H. *Liq. Cryst.* **2005**, *32*, 1005–1012.
(10) Glushchenko A.; Kresse H.; Reshetnyak V.; Reznikov Y.; Yaroshchuk O. *Liq.Cryst.* **1997**, *23*, 241–246.
(11) Zakrevska S.; Zakrevskyy Y.; Nych A.; Yaroshchuk O.; Mashke U. *Mol. Cryst. liq. Cryst.* **2002**, *375*, 467–480.

(12) Zhou B.; Iannacchione G.; Garland C.; Bellini T. *Phys. Rev. E* **1997**, *55*, 2962–2968.
(13) Van Boxtel M.; Wubbenhorst M.; Van Turnhout J.; Bastiaansen C.; Broer D. *Liq. Cryst.* **2003**, *30*, 235–249.
(14) Jones T. *Clay Miner.* **1983**, *18*, 399–410.
(15) Feller J.; Bruzaud S.; Grohens Y. *Mater. Lett.* **2004**, *58*, 739–745.
(16) Bezrodna T.; Chashechnikova I.; Puchkovska G.; Tolochko A.; Shaydyuk Y.; Lebovka N.; Baran J.; Drozd M.; Ratajczak H. *Liq. Cryst.* **2006**, *30*, 1113–1119.
(17) Luckhurst G.; Stephans R.; Phyppen R. *Liq. Cryst.* **1990**, *8*, 451–464.
(18) Bunning T.; Kreuzer F. *TRIP* **1995**, *3*, 318–323.
(19) Ho D.; Briber R.; Glinka C. *Chem. Mater.* **2001**, *13*, 1923–1931.
(20) Lazarev A.N. *Kolebatel'nie Spektri i Stroenie Silikatov*; Nauka: Leningrad, 1968 (in Russian).
(21) Tarasevich Y.I.; Ovcharenko F.D. *Adsorbcija na Glinistih Mineralah*; Naukova dumka: Kiev, 1975 (in Russian).
(22) Sontevska V.; Jovanovski G.; Makreski P. *J. Mol. Struct.* **2007**, *834–836*, 318–327.
(23) Stubican V.; Roy R. *Am. Miner.* **1961**, *46*, 32–51.
(24) Farmer V.; Russell J. *Spectrochim. Acta* **1964**, *20*, 1149–1173.
(25) Russell J.; Farmer V.; Velde B. *Miner. Mag.* **1970**, *37*, 869–879.
(26) Sverdlov L.M.; Kovner M.A.; Krainov E.P. *Kolebatel'nie Spektri Mnogoatomnykh Molekul*; Nauka: Moscow, 1970 (in Russian).
(27) Babkov L.; Gnatyuk I.; Puchkovskaya G.; Truhachev S. *J. Strukt. Himii* **2002**, *43*, 1098–1105 (in Russian).
(28) Gavrilko T.; Mel'nik V.; Moraru V.; Chashechnikova I.; Shaidyuk Y.; Hauser A. *J. appl. Spectrosc.* **2005**, *72*, 887–892.